Structure of ice confined in carbon and silica nanopores

MONIKA JAŻDŻEWSKA[1,2], **MAŁGORZATA ŚLIWIŃSKA-BARTKOWIAK**[1,3,*],
KAMILA DOMIN[1,3], **DOROTA M CHUDOBA**[1,2], **ANATOLY I BESKROVNYI**[2], **DIMITR S NEOV**[2,4]
and KEITH E GUBBINS[5]

[1]Faculty of Physics, Adam Mickiewicz University, 61-614 Poznan, Poland
[2]Frank Laboratory of Neutron Physics, Joint Institute for Nuclear Research, Dubna 141980, Russia
[3]NanoBioMedical Centre, Adam Mickiewicz University, 61-614 Poznan, Poland
[4]Institute for Nuclear Research and Nuclear Energy, Sofia BG-1784, Bulgaria
[5]Department of Chemical and Biomolecular Engineering, NC State University, Raleigh, NC 27695-7905, USA
*Author for correspondence (msb@amu.edu.pl)

Abstract. In this work, water confined in silica and carbon nanopores has been examined. The purpose of this study is to describe the melting behaviour and structure of ice confined in silica nanopores, KIT-6 and ordered carbon nanopores, CMK-3, having pore diameters of 5.9 and 5.2 nm, respectively. To determine the melting temperature of ice inside the nanopores, we performed differential scanning calorimetry measurements of the systems studied. We found that the melting temperature of confined ice is reduced relative to the bulk melting point and this shift is 16 K for water confined in KIT-6 and 21 K for water confined in CMK-3. The structural properties of water at the interfaces were analysed by using the neutron diffraction method (ND). The ND measurements for all the systems studied, showed the features of both hexagonal ice, I_h, and cubic ice, I_c. However, we show that the ice confined in nanopores does not have a structure corresponding to the typical hexagonal form or the metastable cubic form. The ice confined in nanopores has a structure made up of cubic sequences interlaced with hexagonal sequences, which produce the stacking disordered ice (ice I_{sd}).

Keywords. Nanophase; ice structure; carbon and silica nanopores; neutron diffraction; effect of confinement; cubicity.

1. Introduction

The phase diagram of ice shows that they have many different crystal forms; these forms depend on the local molecular correlations that influence the ordered arrangement of hydrogen-bonded configurations. There are 15 crystalline phases of ice [1], 3 polyamorphic states of ice [2] and high viscosity liquid phases [3] that are known. A lot of these structures are high-pressure and low temperature forms of ice.

In general, it is assumed that under ambient conditions, ice exists in two crystalline forms: stable hexagonal ice (ice I_h) and metastable cubic ice (ice I_c). Usually, water freezes to hexagonal ice which crystallizes in the space group $P6_3/mmc$, but under certain conditions, mostly in laboratory, it can freeze to create cubic ice in the space group $Fd3m$ [4]. Both hexagonal and cubic ice consist of layers composed of six-membered rings of hydrogen-bonded water molecules; however, they differ in the arrangement of second-neighbours layer [5].

There are several ways by which ice I_c [6] can be formed [7]. It can be obtained, for example, from vapour deposition [6] and in addition by the warming of amorphous ices [8,9] and recovered high-pressure forms of ice [10,11] and by freezing of nanometre-scale water clusters [12,13]. Recently, the creation of a cubic form of ice by freezing of water confined in nanopores has also been also reported [14–16]. Cubic ice is usually obtained in the form of very small crystallites that lead to particle size broadening of the diffraction pattern [17]. It is considered that sample size (i.e., droplet or pore size) plays an important role in the formation of ice I_c. It was found that transitions starting from a solid water phase which lead to ice I_c are irreversible [7].

Cubic structure or a defective form of cubic ice is usually formed in nanometre-sized confined geometry [15,16,18–24]. Seyed-Yazdi *et al* [25,26] showed that the nucleation of water confined in silica nanopores creates a mixture that incorporates hybrid crystallites of ice I_h and ice I_c with an intermediate density form of amorphous ice. Liu *et al* [18] claimed that in the case of the over-filled sample, the water inside pores freezes to form a defective cubic form of ice, while the formation of a hexagonal structure is observed outside of the silica grains. While using molecular dynamics simulations, Moore *et al* [27] found that the ratio of cubic to hexagonal layers in confined ice is about 2:1. Moreover, the structure of ice confined in hydrophilic nanopores of 3 nm diameter has stacking faults.

It is considered that the formation of cubic structures, rather than hexagonal structures, in the pores can be attributed to the restrictions on the size of the crystallite. However, according

1

to recently published studies [4,10,28–31], the cubic form that has been observed is not exactly cubic. This form of ice, so-called cubic phase, shows stacking faults instead of an ordered arrangement of two-dimensional layers [28]. It is clear that the form of ice which was called cubic ice in the past is, in fact, a stacking-disordered material containing cubic sequences interlaced with hexagonal sequences [31]. Kuhs *et al* [10] noticed that their samples of ice I, which they referred to as ice I_c, contained some deformation faults in the I_c form. These stacking faults are the result of randomly dispersed sequences of hexagonal ice in the structure of cubic ice. Hansen *et al* [17,32] quantitatively showed that all the non-cubic features in ice I, formed from ice V and ice IX, could be the result of the stacking disorder and the so-called cubic ice is not cubic, but trigonal (space group $P3m1$). In previous literature on the subject, we can find two main nomenclatures that have been suggested for stacking disordered ice I. Malkin *et al* [31] proposed the abbreviation ice I_{sd}. This term includes both ice I_c with varying amounts of ice I_h sequences and ice I_h containing varying amounts of ice I_c sequences. Hansen *et al* [33] suggested another term that may be seen as a continuum from ideal ice I_c to ideal ice I_h. They analysed the effect of different stacking disorder interactions on the diffraction patterns of stacking disordered ice and proposed to name it ice I_{ch}. The propensity of ice I to grow with stacking disorders has been observed in a large number of experimental and simulation studies [5,7,15,27,34–41].

It is known that water confined in a nanoscale environment exhibits unique properties and has been the subject of much attention. The behaviour of the nanoconfined phase is different from the behaviour of the bulk phase, which occurs due to the size effect and competition between the fluid–wall and fluid–fluid intermolecular interactions. In the phase transition phenomena it can lead to the decreasing of the melting temperature of adsorbate relative to the bulk melting point [42–47].

2. Methods

We report on the experimental studies of the melting transition and structure of ice confined in silica and cylindrical carbon nanopores of similar inner diameter: 5.9 and 5.2 nm, respectively. The experimental methods used for the studies are: differential scanning calorimetry (DSC) and neutron diffraction (ND).

2.1 *Materials*

In our experiments, we have used silica nanopores of type KIT-6 and mesoporous carbon material CMK-3, which are the reverse carbon replica of silica mesopores, SBA-15. The silica mesopores SBA-15 and KIT-6 were synthesized according to the literature procedure [48,49]. As a carbon precursor, in the case of CMK-3 nanopores, furfuryl alcohol was used [50]. The materials were characterized by several methods
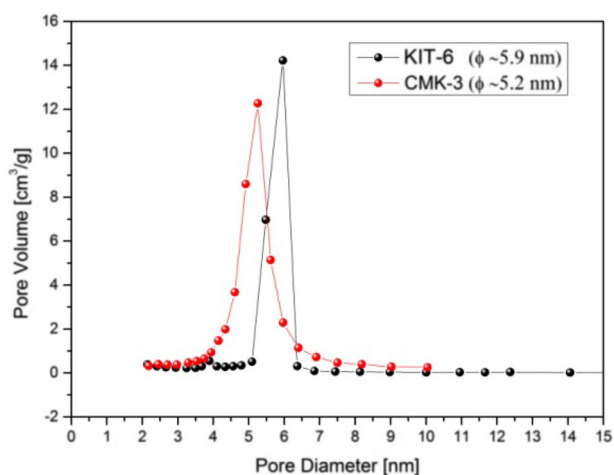

Figure 1. Pore size distribution calculated for the CMK-3 and KIT-6 matrices.

e.g., transmission electron microscopy and small angle X-ray scattering and nitrogen sorption analysis (Micrometrics ASAP 2020). The specific surface area was calculated using the Brunauer–Emmet–Teller (BET) method and pore volume and pore size distribution were derived using the Barrett–Joyner–Halenda (BJH) method [50]. The pore size distributions calculated for the samples of CMK-3 (5.2 nm) and KIT-6 (5.9 nm) are presented in figure 1.

Porous samples were heated to about 400 K and kept under vacuum (10^{-3} torr) for several days to remove air prior to and during the introduction of D_2O (100% deuterium purchased from Sigma) or deionized H_2O water. The samples for ND measurements were then hydrated in a humid atmosphere at room temperature for a few days. The hydrated process was continued until the sample mass increased by about 70%. This way of sample preparation allowed us to obtain samples with D_2O only inside the pores, and there was no excess water outside the pores. For DSC measurements, the carbon materials were filled with deionized water under vacuum by using a special tube. This method of filling the carbon nanopores with water ensured very good pore saturation. As a result, we obtained samples that contained water inside and outside the pores which allowed us to determine the shift of the melting temperature of water in the pores and directly compare it to the bulk melting point.

2.2 *DSC measurements*

The analysed systems were characterized by using DSC and ND methods. The melting behaviour of the confined water was studied by the DSC method. A PerkinElmer DSC 800 advanced double-furnace DSC was used to determine the melting temperature of ice confined in nanopores. The measurements were performed at temperature ranging between 173 and 313 K with a heating rate of 10 K min^{-1}. The

melting temperatures were determined from the position of the peaks of the heat flow signals on a heating thermogram.

2.3 *ND method*

The crystal structure of confined ice was determined by the ND method. D_2O water was used in the neutron scattering study to avoid the complications of incoherent scattering and inelasticity corrections. The ND measurements were performed in the real-time powder diffractometer [51,52] at the Frank Laboratory of Neutron Physics of the Joint Institute for Nuclear Research (JINR) with the fast-pulsed reactor IBR-2. The resolution of the diffraction patterns was determined by the width of the pulse from the neutron source, $\Delta d/d = 0.01$, in the range of interplanar spacings, d_{hkl}, from 1 to 20 Å. The scattering angle, $2\theta = 170°$ was fixed. The sample was placed in a vanadium container with a diameter of 3 mm and a height of 25 mm and was cooled to about 100 K and then warmed to 300 K. Structure refinement was carried out using the FullProf program based on the multi-phase Rietveld analysis method [53,54].

3. Results and discussion

The melting behaviour of water confined in KIT-6 and CMK-3 nanopores was determined using the DSC method. The DSC scans corresponding to the melting of H_2O in silica and carbon pores are presented in figure 2.

The endothermic peaks which occur at the temperature of 257 K in the case of KIT-6 and at 252 K for CMK-3 are related to the melting temperature of the confined ice. We also observed an endothermic peak at a temperature of 273 K which is connected with the bulk melting point of ice. The shift of the melting temperatures towards lower temperatures for H_2O in KIT-6 and CMK-3 mesopores relative to bulk water is -16 and -21 K, respectively ($\Delta T = T_{\text{mbulk}} - T_{\text{mpores}}$).

To determine the structure of confined ice, the ND method was used which provided information on the long-range order in crystal structures. The diffraction spectra indicate whether the studied materials satisfied the Bragg's law. While studying an ordered crystal material, sharp diffraction peaks are observed. When the long-range order in a crystal breaks, it influences the diffraction pattern.

In figure 3, the diffraction patterns for D_2O in KIT-6 and CMK-3 at a temperature of 270 K are presented. At 270 K, we did not observe crystalline peaks (the ice in the pores is in liquid phase), so the diffraction pattern is typical for the amorphous liquid state.

The ND patterns for D_2O water in KIT-6 and CMK-3 at 100 K is presented in figure 4.

Figure 4 shows the crystalline forms of water. The main triplet shows the features of the hexagonal ice with space group $P63/mmc$ and peaks at the positions: $d = 3.90$, 3.66 and 3.44 Å corresponding to the main reflections of planes [100], [002] and [101] for both the studied systems.
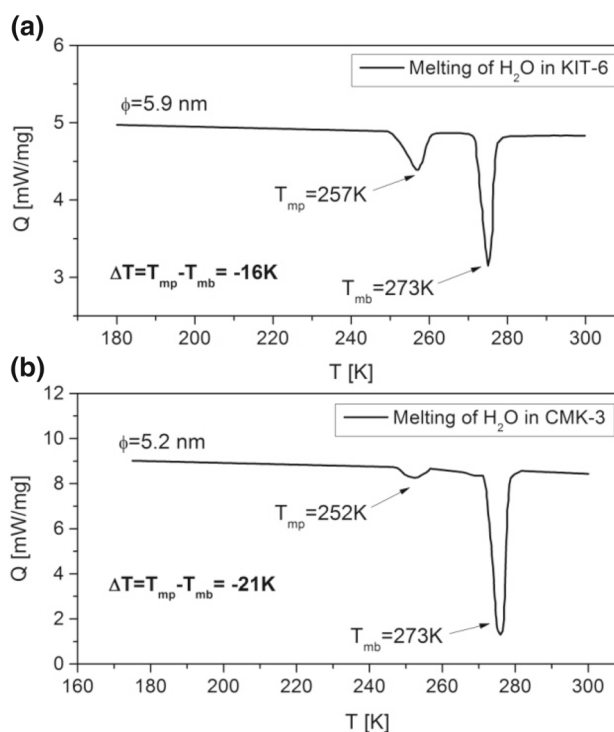

Figure 2. DSC scan for H_2O confined in (**a**) KIT-6 and (**b**) CMK-3 with mesopores of diameter of 5.9 and 5.2 nm, respectively.
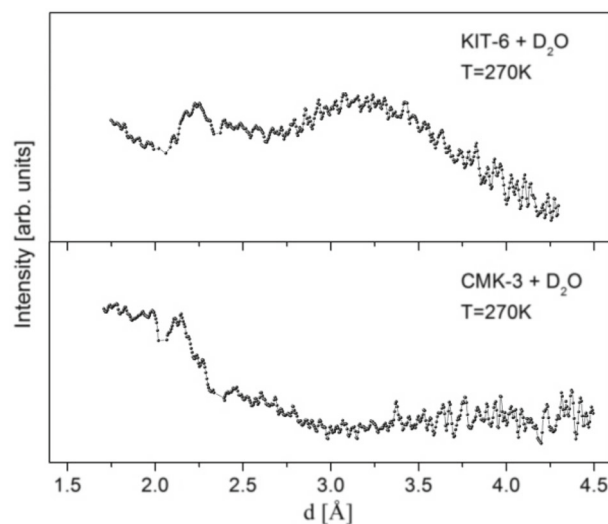

Figure 3. ND results for D_2O in KIT-6 and CMK-3, measured at 270 K.

However, the widths of the observed peaks are broader relatively to the hexagonal crystal structure. In addition, the intensity of the experimental peaks does not correspond to the diffraction pattern for hexagonal ice [18] and does not match the calculated patterns that are shown in figure 5. In table 1, the structural parameters of the hexagonal I_h and cubic I_c phases are presented.
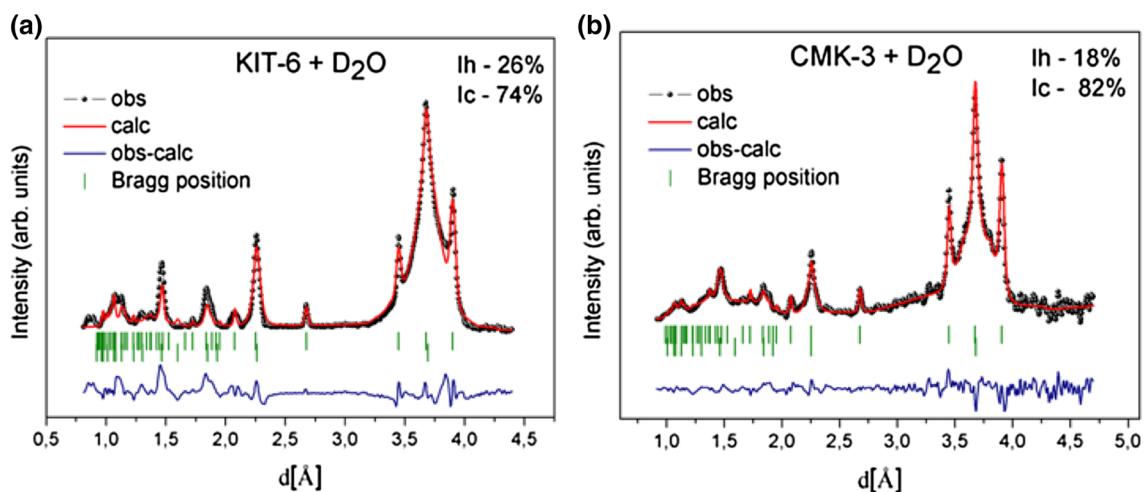
Figure 4. ND patterns and the results of Rietveld refinement of D_2O in (**a**) KIT-6 and (**b**) CMK-3 at $T = 100$ K and the percentage composition of ice I phases (the blue dotted line shows the difference between the experimental spectrum and Rietveld refinement).
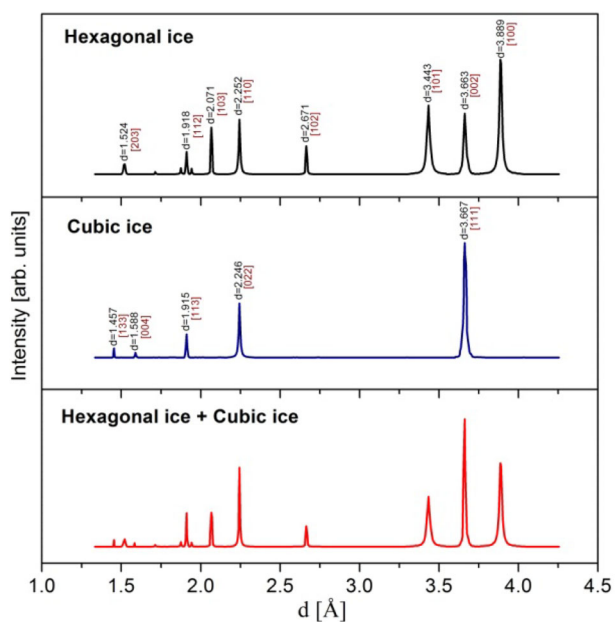

Figure 5. The calculated patterns for (**a**) hexagonal ice structure, (**b**) cubic ice structure and (**c**) superposition of I_h and I_c.

In figure 5a, the diffraction pattern calculated on the basis of the Mincryst Crystallographic Database for hexagonal ice is presented.

In figure 5b, the calculated diffraction pattern for cubic ice with the space group $Fd3m$ is presented and in figure 5c, the superposition of these two forms of ice is shown. In the experimental diffraction patterns shown in figure 4, the peaks in the centre of the triplet ($d = 3.66$ Å) can be a superposition of the cubic and hexagonal ice structures, comparable with the diffraction pattern shown in figure 5c. The peaks in

further positions ($d = 2.24$ and 1.83 Å), which are typical of cubic ice as well as of hexagonal ice structures, also showed a significant broadening when compared with the calculated diffraction patterns, which is suggestive of some disorder in the crystal. As we can see from the experimental profiles (figure 4), the peaks that can be treated as a superposition of the cubic and hexagonal forms of ice ($d = 3.66$, 2.24 and 1.83 Å) are significantly broadened and indicative of a defective structure of ice, which cannot be a simple mixture of cubic and hexagonal ice structures. Such a defective structure of the cubic ice was also observed in previous experiments on confined ice formation [15,18,25]. Recently published results of X-ray diffraction studies for water confined in nanopores [55,56] and the theoretical studies by Malkin *et al* [31,38] suggest that the obtained profile can be a hybrid of both hexagonal and cubic ice forms that were formed as a result of stacking faults. The theory [38] predicts that when a water droplet freezes, a two-dimensional nucleation process occurs. As a result, the layers of hexagonal and cubic ice structures grow alternately in the crystal (in various combinations) and the resulting ice is made up of a combination of intertwined cubic and hexagonal stacking sequences. The name proposed for this complex structure of ice is disordered stacking ice, I_{sd}. It is precisely these faults that lead to the formation of a defective lattice structure.

The FullProf program was used to fit both the intensities and peak positions of the investigated samples. We used this program to assess the contribution of hexagonal ice and cubic ice in I_{sd} for the analysis of the diffraction pattern obtained. We have noticed that the ice confined in pores of KIT-6 contains about 26% hexagonal ice and 74% cubic ice fractions, whereas in the case of ice confined in the pores of CMK-3, we have observed about 18% hexagonal ice and 82% cubic I_c fractions. The Bragg R-factors from the analysis of data were 7.6 (I_h) and 10.8

Table 1.   Structural parameters of hexagonal I_h and cubic I_c phases.

	I_h							
Crystal system	Hexagonal				Cubic			
Space group	$P6_3/mmc$				$Fd\text{-}3m$			
Space group number	194				227			
a (Å)	4.5040				6.3530			
b (Å)	4.5040				6.3530			
c (Å)	7.3337				6.3530			
α (°)	90.0000				90.0000			
β (°)	90.0000				90.0000			
γ (°)	120.0000				90.0000			

	Co-ordinates						
Atoms	x	y	z	x	y	z
D1	0.54680	0.09360	0.51640	0.03300	0.03300	0.03300
D2	0.33333	0.66667	0.19930	—	—	—
O1	0.33333	0.66667	0.06360	0.12500	0.12500	0.12500

Position of peaks (no.)	h	k	l	d (Å)	I (%)	h	k	l	d (Å)	I (%)
1	1	0	0	3.90058	100.0	1	1	1	3.66791	100.0
2	0	0	2	3.66685	53.1	0	2	2	2.24612	47.2
3	1	0	1	3.44378	60.4	1	1	3	1.91550	20.2
4	1	0	2	2.67166	24.6	2	2	2	1.83395	0.2
5	1	1	0	2.25200	47.6	0	0	4	1.58825	4.1
6	1	0	3	2.07139	40.8	1	3	3	1.45748	7.9
7	2	0	0	1.95029	4.9					
8	1	1	2	1.91899	19.6					
9	2	0	1	1.88478	5.4					
10	0	0	4	1.83343	0.1					
11	2	0	2	1.72189	2.0					
12	1	0	4	1.65927	0.1					
13	2	0	3	1.52455	8.8					
14	2	1	0	1.47428	3.2					
15	2	1	1	1.44536	2.5					
16	1	1	4	1.42181	0.1					
17	1	0	5	1.37289	5.0					
18	2	1	2	1.36786	2.0					
19	2	0	4	1.33583	0.1					

(I_c) for CMK-3 and 7.9 (I_h) and 16.9 (I_c) in the case of KIT-6. In figure 4, the Rietveld refinement for D_2O in KIT-6 (figure 4a) and CMK-3 (figure 4b) at $T = 100$ K and the percentage composition of the phases (cubic and hexagonal ice) are presented.

As can be seen from figure 4, for D_2O in KIT-6, we observed the presence of 74% of the cubic phase and 26% of the hexagonal phase ice fractions and for D_2O in CMK-3, we observed 82% of the cubic phase and 18% of the hexagonal phase fractions. Our results showed that the cubicity depends on the kind of pore walls as the pore sizes are similar for both porous matrices. We can see that the silica pores are more preferential for the hexagonal ice formation than the carbon walls of the pores. The relationship between the cubicity of ice I and the corresponding degree of stacking disorder should be taken into consideration when analysing the structure of ice. According to Carr *et al* [5], the highest stacking disorder state is reached at cubicity of 50% in ice. When the ratio of cubic ice increases relative to hexagonal ice, the stacking disorder decreases until the perfect I_c structure is attained, when I_c is free of any stacking disorders. Also, in pure ice I_h, when the cubicity is zero, there is no stacking disorder present. It was found that the small size of drops can play a role in increasing cubicity. Ice confined in nanopores becomes more cubic as the pore size decreases [14,15]. A similar dependence was shown by Domin *et al* [55]; when water is confined in smaller pores, the calculated percentage composition of the cubic form of ice increases. Malkin *et al* [38] showed that

the ice produced from homogeneous nucleation in pure water droplets at around 230 K was fully random, with 50% cubic and 50% hexagonal stackins. Hansen *et al* [32] were able to show the probabilities of occurrence of cubic and hexagonal sequences in ice formed from ice V and ice IX. These probabilities show that cubic sequences are present up to ~60% in ice I_{sd} formed from ice V. They also indicated that the correlations between stacking faults are different depending on the route of formation. Furthermore, Moore *et al* [27] showed that the number of cubic layers of ice in the pores is much higher that the number of hexagonal layers. On the basis of our study, we were able to show that in the confined space, the type of pore surfaces (silica and carbon) can control the ratio of the cubic and hexagonal ice in I_{sd} ice, even in the case where pore sizes are very similar.

4. Conclusion

Our DSC results indicated a reduction in the melting temperature of water confined in the ordered silica and carbon mesopores. This effect can be explained in terms of the fluid–wall attractive interaction and agrees with previous results [42–47]. ND research, which was made at temperatures below the pore melting temperature, provides a strong evidence of the presence of both hexagonal and cubic ice inside the pores. We were not able to obtain a good Rietveld refinement of our diffraction patterns with typical hexagonal and cubic separated ice forms. Our diffraction data show the existence of features (such as diffraction profile broadening) of stacking disorder ice I_{sd} confined in pores. The asymmetric profile that has been associated with the presence of some defects or disorders in the confined ice structure was also observed in previous studies which concern the ice in nanopores [23,25,26,55]. We evaluated the percentage contribution of cubic and hexagonal ice inside silica and carbon mesopores. The results showed a higher contribution of the cubic form in the case of carbon pores compared with the silica pores, which is related to the degree of disordering of the crystal structure.

Knowledge of the process of formation of stacking faults, which are a type of disorder at a nanometre scale in crystals, is crucial for the production of technologically important materials, whose properties significantly depend on such a disorder.

Acknowledgements

References

[1] Salzmann C G, Radaelli P G, Slater B and Finney J L 2011 *Phys. Chem. Chem. Phys.* **13** 18468

[2] Loerting T, Winkel K, Seidl M, Bauer M, Mitterdorfer C, Handle P H *et al* 2011 *Phys. Chem. Chem. Phys.* **13** 8783

[3] Palmer J C, Martelli F, Liu Y, Car R, Panagiotopoulos A Z and Debenedetti P G 2014 *Nature* **510** 385

[4] Johari G P and Andersson O 2015 *J. Chem. Phys.* **143** 054505

[5] Carr T H G, Shephard J J and Salzmann C G 2014 *J. Phys. Chem. Lett.* **5** 2469

[6] König H 1943 *Z. Kristallogr.* **105** 279

[7] Kuhs W F, Sippel C, Falenty A and Hansen T C 2012 *Proc. Natl. Acad. Sci.* **109** 21259

[8] Dowell L G and Rinfret A P 1960 *Nature* **188** 1144

[9] Mcmillan J A and Los S C 1965 *Nature* **206** 806

[10] Kuhs W F, Bliss D V and Finney J L 1987 *J. Phys. Colloq.* **48** 631

[11] Bertie J E, Calvert L D and Whalley E 1963 *J. Chem. Phys.* **38** 840

[12] Huang J and Bartell LS 1995 *J. Chem. Phys.* **99** 3924

[13] Bartell L S and Lennon P L 2009 *J. Chem. Phys.* **130** 084303

[14] Morishige K, Yasunaga H and Uematsu H 2009 *J. Phys. Chem. C* **113** 3056

[15] Morishige K and Uematsu H 2005 *J. Chem. Phys.* **122** 44711

[16] Steytler D C, Dore J C and Wright C J 1983 *J. Phys. Chem.* **87** 2458

[17] Hansen T C, Koza M M and Kuhs W F 2008 *J. Phys. Condens. Matter* **20** 285104

[18] Liu E, Dore J C, Webber J B W, Khushalani D, Jahnert S, Findenegg G H *et al* 2006 *J. Phys. Condens. Matter* **18** 10009

[19] Dunn M, Dore J C and Chieux P 1988 *J. Cryst. Growth* **92** 233

[20] Dore J, Webber B, Hartl M, Behrens P and Hansen T 2002 *Physica A* **314** 501

[21] Baker J M, Dore J C and Behrens P 1997 *J. Chem. Phys.* **101** 6226

[22] Handa Y P, Zakrzewski M and Fairbridge C 1992 *J. Phys. Chem.* **96** 8594

[23] Dore J 2000 *Chem. Phys.* **258** 327

[24] Takamuku T, Yamagami M, Wakita H, Masuda Y and Yamaguchi T 1997 *J. Phys. Chem. B* **101** 5730

[25] Seyed-Yazdi J, Farman H, Dore J C, Webber J B W and Findenegg G H 2008 *J. Phys. Condens. Matter* **20** 205108

[26] Seyed-Yazdi J, Farman H, Dore J C, Webber J B W, Findenegg G H and Hansen T 2008 *J. Phys. Condens. Matter* **20** 205107

[27] Moore E B, Llave E, Welke K, Scherlis D A and Molinero V 2010 *Phys. Chem. Chem. Phys.* **12** 4124

[28] Fitzgerald R J 2013 *Phys. Today* **66** 16

[29] Amaya A J, Pathak H, Modak V P, Laksmono H, Loh N D, Sellberg J A *et al* 2017 *J. Phys. Chem. Lett.* **8** 3216

[30] Lupi L, Hudait A, Peters B, Grünwald M, Mullen R G, Nguyen A H *et al* 2017 *Nature* **551** 218

[31] Malkin T L, Murray B J, Salzmann C G, Molinero V, Pickering S J and Whale T F 2015 *Phys. Chem. Chem. Phys.* **17** 60

[32] Hansen T C, Koza M M, Lindner P and Kuhs W F 2008 *J. Phys. Condens. Matter* **20** 285105

[33] Hansen T C, Sippel C and Kuhs W F 2015 *Z. Kristallogr.* **230** 75

[34] Hansen T C, Falenty A and Kuhs W F 2007 in *Physics and chemistry of ice* W F Kuhs (ed.) (Cambridge: Royal Society of Chemistry) p 201

[35] Kuhs W F, Genov G, Staykova D K and Hansen T 2004 *Phys. Chem. Chem. Phys.* **6** 4917

[36] Kohl I, Mayer E and Hallbrucker A 2000 *Phys. Chem. Chem. Phys.* **2** 1579

[37] Hudait A, Qiu S, Lupi L and Molinero V 2016 *Phys. Chem. Chem. Phys.* **18** 9544

[38] Malkin T L, Murray B J, Brukhno A V, Anwar J and Salzmann C G 2012 *Proc. Natl. Acad. Sci.* **109** 1041

[39] Moore E B and Molinero V 2011 *Phys. Chem. Chem. Phys.* **13** 20008

[40] González Solveyra E, Llave E, Scherlis D A and Molinero V 2011 *J. Phys. Chem. B* **115** 14196

[41] Johnston J C and Molinero V 2012 *J. Am. Chem. Soc.* **134** 6650

[42] Alba-Simionesco C, Coasne B, Dosseh G, Dudziak G, Gubbins K E, Radhakrishnan R *et al* 2006 *J. Phys. Condens. Matter* **18** R15

[43] Gelb L D, Gubbins K E, Radhakrishnan R and Sliwinska-Bartkowiak M 1999 *Rep. Prog. Phys.* **62** 1573

[44] Radhakrishnan R, Gubbins K E and Sliwinska-Bartkowiak M 2002 *J. Chem. Phys.* **116** 1147

[45] Sliwinska-Bartkowiak M, Dudziak G, Sikorski R, Gras R, Radhakrishnan R and Gubbins K E 2001 *J. Chem. Phys.* **114** 950

[46] Morishige K, Yasunaga H and Matsutani Y 2010 *J. Phys. Chem. C* **114** 4028

[47] Sliwinska-Bartkowiak M, Jazdzewska M, Huang L L and Gubbins K E 2008 *Phys. Chem. Chem. Phys.* **10** 4909

[48] Jun S, Joo S H, Ryoo R, Kruk M, Jaroniec M, Liu Z *et al* 2000 *J. Am. Chem. Soc.* **122** 10712

[49] Kleitz F, Choi S H and Ryoo R 2003 *Chem. Commun.* **17** 2136

[50] Domin K 2016 PhD thesis (A. Mickiewicz University)

[51] Balagurov A M, Beskrovnyy A I, Zhuravlev V V, Mironova G M, Bobrikov I A, Neov D *et al* 2016 *J. Surf. Invest.: X-ray, Synchrotron Neutron Tech.* **10** 467

[52] Real-Time Neutron Diffractometer. Available: http://flnph.jinr.ru/en/facilities/ibr-2/instruments/dn-2

[53] Rietveld H M 1969 *J. Appl. Cryst.* **2** 65

[54] Zlokazov V B and Chernyshev V V 1992 *J. Appl. Cryst.* **25** 447

[55] Domin K, Chan K Y, Yung H, Gubbins K E, Jarek M, Sterczynska A *et al* 2016 *J. Chem. Eng. Data* **61** 4252

[56] Suzuki Y, Duran H, Steinhart M, Kappl M, Butt H J and Floudas G 2015 *Nano Lett.* **15** 1987